Vibration analysis of a misaligned rotor–coupling–bearing system passing through the critical speed

S Prabhakar, A S Sekhar* and **A R Mohanty**
Department of Mechanical Engineering, Indian Institute of Technology, Kharagpur, India

Abstract: The transient response of a misaligned rotor–coupling–bearing system passing through the critical speed has been analysed by using the finite element method (FEM) for flexural vibrations. The coupling has been modelled in two ways: a frictionless joint and a joint with stiffness and damping. From the vibration analysis, the subcritical speeds at one-half, one-third and one-fourth the critical speed have been found when the misaligned rotor–coupling–bearing system passes through its critical speed. The continuous wavelet transform (CWT) has been used as a tool to extract the silent features from the time response of the rotor system. A parametric study has been carried out to investigate the transient response of this rotor system for different angular accelerations in different types of misalignment.

Keywords: vibration, rotor, coupling, bearing, critical speed, finite element method

NOTATION

a	angular acceleration of the rotor system
$\bar{d}_a$	external damping coefficient of the coupling joint
$\bar{d}_i$	internal damping coefficient of the coupling joint
D	shaft diameter
$[\mathbf{D}]$	matrix including gyroscopic effects and damping
e	unbalance eccentricity of the rotor
E	modulus of elasticity
$FX1, FX2, \ldots$	reaction forces
I_D	diametral moment of inertia
I_P	polar moment of inertia
$\bar{k}$	rotational spring stiffness of the coupling joint
K_a	axial spring rate per disc pack
K_b	bending spring rate per degree per disc pack
$[\mathbf{K}_{f1}]$	stiffness matrix of a coupling having a frictionless joint
$[\mathbf{K}_{f2}]$	stiffness matrix of a coupling having a joint with stiffness and damping
l	element length
L	length of the rotor
M	bending moment
$[\mathbf{M}]$	mass matrix
$\{\boldsymbol{q}\}$	vector of nodal quantities
$\{\boldsymbol{Q}\}$	force vector
t	time
Tq	torque
$\Delta X, \Delta Y, \ldots$	misalignment displacements
Z_3	centre of articulation
ΔZ	stretch (+) or compression (−) of the complete coupling from its free length
β	angle in the x direction at the coupling joint as well as at other nodes
γ	angle in the y direction at the coupling joint as well as at other nodes
θ_1	$\sin^{-1}(\Delta X1/Z_3)$
θ_2	$\sin^{-1}(\Delta X2/Z_3)$
θ_3	misalignment angle
ϕ_1	$\sin^{-1}(\Delta Y1/Z_3)$
ϕ_2	$\sin^{-1}(\Delta Y2/Z_3)$
φ	instantaneous operating speed
ω_c	critical speed
Ω	operating speed

The MS was received on 23 March 2001 and was accepted after revision for publication on 20 July 2001.
**Corresponding author: Department of Mechanical Engineering, Indian Institute of Technology, Kharagpur 721 302, India.*

1 INTRODUCTION

In industrial rotor–bearing systems, rotor unbalance and shaft-to-shaft misalignment are two common and principal sources of vibration that are of major concern. A number of analytical methods have been applied to calculate unbalance response, and this is well understood. However, limited research has been done on the vibrational characteristics of rotor systems that are due to shaft-to-shaft misalignment.

Downloaded from pic.sagepub.com at COLUMBIA UNIV on February 3, 2015

Shaft misalignment is a condition in which the shafts of the driving and driven machines are not on the same centre-line. Perfect alignment between the driving and driven machines cannot be attained in practice. Even if perfect alignment is achieved initially, it cannot be maintained during operation of the machine owing to various factors such as the differential thermal growth of machines, piping forces caused by either temperature change or pressure change, foundation movement, etc. Thus, a misalignment condition is virtually always present in the machine trains. Therefore, flexible couplings are used to accommodate the existing misalignment between driving and driven shafts and to transmit rotary power without torsional slip.

A great deal of work has been done on couplings, as reported in the review by Xu and Marangoni [**1**]. However, little literature is available on coupling misalignment (shaft to shaft), in spite of its importance in the industrial world. Rivin [**2**] proposed the classification of couplings as rigid, misalignment compensating, torsionally flexible and combination purpose. The effect of coupling geometry, mass and location and the coupling mass unbalance level on lateral vibrations of machines has been studied by Woodcock [**3**].

Misalignment of machinery shafts causes reaction forces and moments to be generated in the coupling which are often a major cause of machinery vibration. Gibbons [**4**] has given the forces and moments acting at the coupling centres of articulation for different types of coupling in the presence of parallel misalignment. Arumugam *et al.* [**5**] modelled the reaction forces and moments for combined parallel and angular misaligned flexible coupling. Sekhar and Prabhu [**6**] have developed a higher-order finite element with eight degrees of freedom per node for a misaligned rotor–coupling–bearing system and numerically evaluated the effects of coupling misalignment on the double vibration response of a rotor–coupling–bearing system. Dewell and Mitchell [**7**] determined the expected vibration frequencies for a misaligned metallic disc flexible coupling on the basis of an analysis of the structural vibrations produced by misalignment. Several investigators [**8**, **9**] have provided vibration identification charts which indicate that coupling misalignment generally produces twice the shaft speed frequency component. Xu and Marangoni [**10**, **11**] showed that vibration responses due to coupling misalignment mainly occur at the even integer multiples of the rotational speed. Recently, Sekhar and Srinivasa Rao [**12**, **13**] analysed vibrations due to misalignment in a rotor–bearing system with flexible coupling. Lee and Lee [**14**] derived a dynamic model for misaligned rotor–ball bearing systems driven through a flexible coupling by treating the reaction loads and deformations at the bearing and coupling elements as the misalignment effect.

Most of the previous work focused on the steady state vibrations of a misaligned rotor–coupling–bearing system. Vibration monitoring during start-up or shutdown is as important as steady state to detect coupling misalignment, especially for machines such as aircraft engines which start and stop quite frequently and run at high speeds. However, research on the transient responses of vibrations of a misaligned rotor–coupling–bearing system passing through the critical speed is rarely found in the literature, to the best of the authors' knowledge.

The vibration signals during machine start-up or rundown are non-stationary (frequency changes with time) in nature. Fourier transform gives the spectral content of the signal, but it gives no information regarding where in time those spectral components appear. On the other hand, wavelets provide time-scale information of a signal, enabling the extraction of features that vary in time. This property makes 'wavelets' an ideal tool for analysing signals of a transient or non-stationary nature. Newland [**15**, **16**] presented the theory of orthogonal wavelets and their application to signal analysis. Staszewski [**17**] has given various wavelet methodologies for damage detection, with some application examples. Wang and McFadden [**18**] have suggested the Gaussian-enveloped oscillating wavelet to detect gear faults. Recently, the continuous wavelet transform (CWT) has been suggested by the authors to detect cracks in a rotor–bearing system while passing through the critical speed [**19**]. Similarly, CWT application on transient analysis of a misaligned rotor–coupling system becomes necessary, considering the fact that very few works are reported on coupling misalignment.

In the present study, the transient analysis of a rotor–coupling–bearing system with coupling misalignment (shaft to shaft) and unbalance has been studied by using the finite element method (FEM) for flexural vibrations. Two different flexible couplings have been modelled for the analysis. The CWT has been used as a tool to extract the silent features of coupling misalignment in a rotor–coupling–bearing system from the time domain signals.

2 SYSTEM EQUATION OF MOTION

Nelson and McVaugh [**20**] have developed the dynamic modelling of rotor–bearing systems by using finite elements. Ozguven and Ozkan [**21**] presented an extended model by synthesizing the previous models. The present study uses these models [**20**, **21**] neglecting shaft internal damping.

The rotor–coupling–bearing system is discretized into finite beam elements as shown in Fig. 1a. A typical shaft rotor element is illustrated in Fig. 1b. The element time-dependent cross-section displacements $(V, W, \mathrm{B}, \Gamma)$ are functions of position, s, along the axis of the element. Each element has two translational and two rotational degrees of freedom for the bending mode at each node represented by q_1 to q_8.

Downloaded from pic.sagepub.com at COLUMBIA UNIV on February 3, 2015

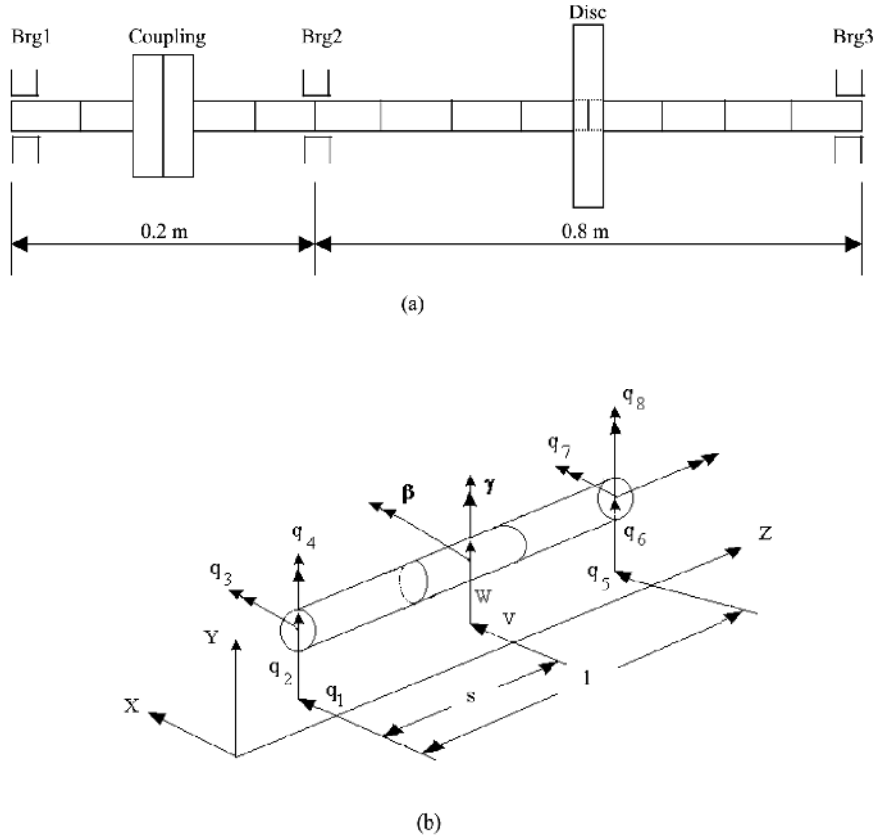

Fig. 1 Rotor–coupling–bearing system with a typical finite rotor element and its coordinates

The equation of motion of the complete rotor system in a fixed coordinate system can be written as

$$[\mathbf{M}]\{\ddot{\boldsymbol{q}}\} + [\mathbf{D}]\{\dot{\boldsymbol{q}}\} + [\mathbf{K}]\{\boldsymbol{q}\} = \{\boldsymbol{Q}\} \tag{1}$$

where mass matrix [**M**] includes the rotary and translational mass matrices of the shaft, the mass and diametral moments of the rigid disc and the flexible coupling. Matrix [**D**] includes the gyroscopic moments, coupling joint damping and the bearing damping. The stiffness matrix considers the stiffness of the shaft elements including the coupling element and the bearing stiffness. The details of the individual matrices of equation (1), except for the coupling element, are given in references [**20**] and [**21**].

The excitation matrix $\{\boldsymbol{Q}\}$ in equation (1) consists of the unbalance forces due to the disc having mass m and eccentricity e, the weight of the disc and reaction forces due to coupling misalignment. The reaction forces due to coupling misalignment are given in Section 4. The unbalance force components in the x and y directions for angular rotation θ are given as

$$F_x = me\{\ddot{\theta}\sin\theta + \dot{\theta}^2\cos\theta\} \tag{2}$$

$$F_y = me\{-\ddot{\theta}\cos\theta + \dot{\theta}^2\sin\theta\} \tag{3}$$

3 MODELLING OF THE FLEXIBLE COUPLING

Modelling of the flexible coupling as discussed by Kramer [**22**] is utilized in the present study. Two technical possibilities will arise while modelling the flexible couplings, namely a frictionless joint or a joint with stiffness and damping.

3.1 Frictionless joint

For a frictionless radially stiff joint, the displacement at the two sides of the joint are identical and angles are different. Figure 2a shows the coordinates of the two

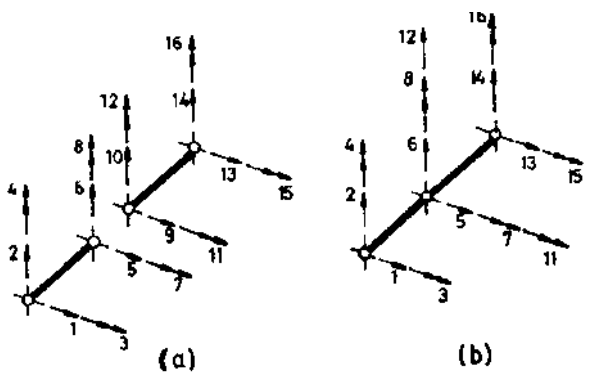

Fig. 2 Coordinates of the two joined elements

Downloaded from pic.sagepub.com at COLUMBIA UNIV on February 3, 2015

shaft elements that are to be joined. With $q_9 = q_5$ and $q_{10} = q_6$, the new coordinates are shown in Fig. 2b for the elements when joined together. Then the stiffness matrix for this case can be written as

$$[\mathbf{K}_{f1}] = \frac{EI}{l^3}\begin{bmatrix}
12 & & & & & & & & & & & & & \\
0 & 12 & & & & & & & & & & & & \\
0 & -6l & 4l^2 & & & & & & & & & & & \\
6l & 0 & 0 & 4l^2 & & & & & & & & & & \\
-12 & 0 & 0 & -6l & 24 & & & & & & & & & \\
0 & -12 & 6l & 0 & 0 & 24 & & & & & & & & \\
0 & -6l & -2l^2 & 0 & 0 & -6l & -4l^2 & & & & & & & \\
6l & 0 & 0 & 2l^2 & 6l & 0 & 0 & 4l^2 & & & & & & \\
0 & 0 & 0 & 0 & 0 & 0 & 0 & 6l & 4l^2 & & & & & \\
0 & 0 & 0 & 0 & 0 & 0 & 6l & 0 & 0 & 4l^2 & & & & \\
0 & 0 & 0 & 0 & 0 & 0 & -12 & 0 & 0 & -6l & 12 & & & \\
0 & 0 & 0 & 0 & 0 & 0 & 0 & -12 & 6l & 0 & 0 & 12 & & \\
0 & 0 & 0 & 0 & 0 & 0 & 0 & -6l & 2l^2 & 0 & 0 & -6l & 4l^2 & \\
0 & 0 & 0 & 0 & 0 & 0 & 0 & 6l & 0 & 0 & 2l^2 & 6l & 0 & 4l^2
\end{bmatrix}$$

Symmetric

3.2 Joint with stiffness and damping

In this coupling joint also, the displacements at the two sides of the joint are identical and angles are different. However, the moments at the coupling joint are to be considered in this case [**22**]. The forces are developed in the flexing elements of the coupling because of the different angles at the two sides of the coupling joint. Hence, the moments are induced at the joint owing to the forces of the flexing elements and the difference angles at the joint. Using the coordinates of Fig. 2 and the difference angles $\beta = \beta_7 - \beta_{11}$, $\gamma = \gamma_8 - \gamma_{12}$ (see Fig. 1 and the notation for the angles), the components of bending moments [**22**] at the coupling joint can be written as

$$M_7 = \bar{k}(\beta_7 - \beta_{11}) + \bar{d}_i\varphi(\gamma_8 - \gamma_{12}) + (\bar{d}_a + \bar{d}_i)(\dot{\beta}_7 - \dot{\beta}_{11}) \tag{4}$$

$$M_8 = -\bar{d}_i\varphi(\beta_7 - \beta_{11}) + \bar{k}(\gamma_8 - \gamma_{12}) + (\bar{d}_a + \bar{d}_i)(\dot{\gamma}_8 - \dot{\gamma}_{12}) \tag{5}$$

$$M_{11} = \bar{k}(\beta_{11} - \beta_7) + \bar{d}_i\varphi(\gamma_{12} - \gamma_8) + (\bar{d}_a + \bar{d}_i)(\dot{\beta}_{11} - \dot{\beta}_7) \tag{6}$$

$$M_{12} = -\bar{d}_i\varphi(\beta_{11} - \beta_7) + \bar{k}(\gamma_{12} - \gamma_8) + (\bar{d}_a + \bar{d}_i)(\dot{\gamma}_{12} - \dot{\gamma}_8) \tag{7}$$

The above equations can be written in matrix form as

$$\{\boldsymbol{f}\} = [\mathbf{K}_1]\{\boldsymbol{q}\} + [\mathbf{D}_1]\{\dot{\boldsymbol{q}}\} \tag{8}$$

where

$$\{\boldsymbol{f}\} = (M_7, M_8, M_{11}, M_{12})^{\mathrm{T}}$$

$$\{\boldsymbol{q}\} = (\beta_7, \gamma_8, \beta_{11}, \gamma_{12})^{\mathrm{T}}$$

$$[\mathbf{K}_1] = \begin{bmatrix} [\mathbf{k}] & -[\mathbf{k}] \\ -[\mathbf{k}] & [\mathbf{k}] \end{bmatrix}, \qquad [\mathbf{k}] = \begin{bmatrix} \bar{k} & \bar{d}_i\varphi \\ -\bar{d}_i\varphi & \bar{k} \end{bmatrix}$$

$$[\mathbf{D}_1] = \begin{bmatrix} [\mathbf{d}] & -[\mathbf{d}] \\ -[\mathbf{d}] & [\mathbf{d}] \end{bmatrix}, \qquad [\mathbf{d}] = \begin{bmatrix} \bar{d}_a + \bar{d}_i & 0 \\ 0 & \bar{d}_a + \bar{d}_i \end{bmatrix}$$

Downloaded from pic.sagepub.com at COLUMBIA UNIV on February 3, 2015

The external damping coefficient, $\bar{d}_a$, is not considered in the present study. For the connected elements as shown in Fig. 2b, the stiffness matrix of this second type of coupling joint, $[\mathbf{K}_{f2}]$, can be obtained by including the $[\mathbf{K}_1]$ matrix at the corresponding degrees of freedom. Matrix $[\mathbf{D}_1]$ is included in matrix $[\mathbf{D}]$ of equation (1) at the corresponding degrees of freedom. The present study utilizes both cases of coupling joints and incorporates the forces and moments due to coupling misalignment at the respective nodes, which is discussed in the following section.

4 COUPLING MISALIGNMENT

Shaft misalignment is a condition in which the components that are coaxial by design are not actually coaxial, either because of assembly errors or on account of deformation of subunits and/or their functions. There are two basic types of shaft misalignment, parallel and angular, as given in reference [**10**]. However, in real situations, shaft misalignment is a combination of both parallel and angular types in the vertical and horizontal directions. However, in the present work only the two basic types of misalignment have been considered for analysis.

Misalignment of machinery shafts causes reaction forces to be generated in the coupling which in turn affect the machines and are often a major cause of vibration. Hence, flexible couplings are necessary to connect the rotating machines to their drives or loads in order to accommodate the unavoidable misalignment of machines. Gibbons [**4**] derived the reaction forces and moments that are developed on account of parallel misalignment. The reaction forces and moments that are developed on account of angular and combined (angular and parallel) misalignment are derived in references [**5**] and [**6**]. The details are presented here as these are introduced in the present work. Figure 3 shows two machine shaft centre-lines, $Z1$ and $Z2$, which are misaligned. The centre-line of the coupling spacer is shown connecting the two shaft centrelines, with intersection points being the coupling centres of articulation, not the shaft ends. The values and the directions of displacements $\Delta X1$, $\Delta Y1$, $\Delta X2$ and $\Delta Y2$ in Fig. 3 can be obtained from the graphical plot of reverse indicator readings. For a machine in the planning stage, realistic values can be chosen for comparative calculations [**4**].

Assuming that $Z1$ is the axis of the driving machine, that (+) torque is applied as shown in Fig. 3 and that the rotation is in the same direction as the applied torque, the reaction forces and moments that the coupling exerts on the machine shafts are as follows [**6**]:

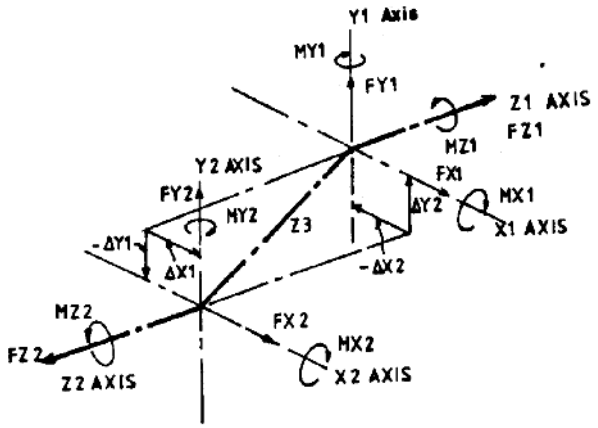

(a) parallel misalignment [4]

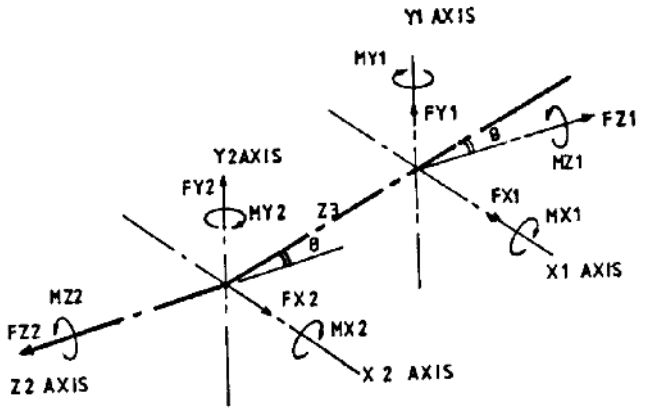

(b) angular misalignment [6]

Fig. 3 Coupling coordinate system: (a) parallel misalignment; (b) angular misalignment

Parallel misalignment:

$$MX1 = Tq \sin\theta_1 + K_b\phi_1,$$

$$MY1 = Tq \sin\phi_1 - K_b\theta_1, \qquad MZ1 = Tq$$

$$MX2 = Tq \sin\theta_2 - K_b\phi_2,$$

$$MY2 = Tq \sin\phi_2 + K_b\theta_2, \qquad MZ2 = -Tq$$

$$FX1 = (-MY1 - MY2)/Z3,$$

$$FY1 = (MX1 + MX2)/Z3,$$

$$FZ1 = K_a\Delta Z + K_a(\Delta Z)^3$$

$$FX2 = -FX1, \qquad FY2 = -FY1, \qquad FZ2 = FZ1$$

Downloaded from pic.sagepub.com at COLUMBIA UNIV on February 3, 2015

Angular misalignment:

$$MX1 = 0.0, \qquad MY1 = 0.0, \qquad MZ1 = Tq/\cos\theta_3$$

$$MX2 = -K_b\theta_3, \qquad MY2 = Tq\sin\theta_3,$$

$$MZ2 = -Tq$$

$$FX1 = (-MY1 - MY2)/Z3,$$

$$FY1 = (MX1 + MX2)/Z3,$$

$$FZ1 = K_a\Delta Z + K_a(\Delta Z)^3/\cos\theta_3$$

$$FX2 = -FX1, \qquad FY2 = -FY1, \qquad FZ2 = FZ1$$

In the present analysis, linear spring rates for the flexural couplings in both bending and axial nodes are assumed. Hence, the term $(\Delta Z)^3$ is neglected in the above expressions for this analysis.

The misalignment moments and the reaction forces are static loads to the non-rotating observer. However, they are acting as periodic loads on the rotating shafts, with a periodic half-sinusoidal function having a time period of π/Ω as given in reference [**5**]. In the present analysis, 1Ω, 2Ω, 3Ω and 4Ω components of the reaction forces are considered and they are incorporated into the excitation matrix $\{\boldsymbol{Q}\}$ in equation of motion (1) at the corresponding degrees of freedom. The nodal force vectors at the corresponding nodes that are due to coupling misalignment are given as

$$\{\boldsymbol{Q}_c^1\} = \begin{Bmatrix} FX1\sin\Omega t + FX1\sin 2\Omega t \\ \quad + FX1\sin 3\Omega t + FX1\sin 4\Omega t \\ FY1\cos\Omega t + FY1\cos 2\Omega t \\ \quad + FY1\cos 3\Omega t + FY1\cos 4\Omega t \\ 0 \\ 0 \end{Bmatrix} \tag{9}$$

$$\{\boldsymbol{Q}_c^2\} = \begin{Bmatrix} FX2\sin\Omega t + FX2\sin 2\Omega t \\ \quad + FX2\sin 3\Omega t + FX2\sin 4\Omega t \\ FY2\cos\Omega t + FY2\cos 2\Omega t \\ \quad + FY2\cos 3\Omega t + FY2\cos 4\Omega t \\ 0 \\ 0 \end{Bmatrix} \tag{10}$$

where $\{\boldsymbol{Q}_c^1\}$ and $\{\boldsymbol{Q}_c^2\}$ are the nodal force vectors at the left and right side of the coupling.

5 CONTINUOUS WAVELET TRANSFORM

In recent times a great deal of interest has been shown in the application of wavelets, and they have been successfully implemented in many fields. Wavelets provide time-scale information of a signal, enabling the extraction of features that vary in time. This property makes 'wavelets' an ideal tool for analysing signals of a transient or non-stationary nature. The continuous wavelet transform (CWT) of $f(t)$ is a time-scale method of signal processing that can be defined as the sum over all time of the signal multiplied by scaled, shifted versions of the wavelet function $\psi(t)$. Mathematically,

$$\text{CWT}(s, b) = \frac{1}{\sqrt{|s|}}\int_{-\infty}^{\infty} f(t)\psi^*\left(\frac{t-b}{s}\right)\mathrm{d}t \tag{11}$$

where $\psi(t)$ denotes the mother wavelet. Parameter s represents the scale index which is a reciprocal of frequency. Parameter b indicates the time shifting (or translation).

The CWT provides the time–frequency information of the signal. This means that any non-stationary events can be localized in time, unlike Fourier analysis. Additionally, the frequency content of these events can be described for any position on the time axis. This property of CWT has been used in the present study to extract significant characteristics that are embedded in time domain signals of the misaligned rotor–coupling–bearing system when passing through its critical speed.

6 RESULTS AND DISCUSSION

A rotor–coupling–bearing system as shown in Fig. 1 has been considered in the present analysis. The analysis has been carried out using FEM for flexural vibrations with parallel and angular misalignments of flexible couplings for two technical possibilities, namely a frictionless joint and a joint with stiffness and damping. Table 1 shows the data used for a rotor–coupling–bearing system with critical speeds for the above two cases. The rotor system is discretized into ten finite elements. Using the flexible coupling modelling in Section 3 and misalignment forces and moments in Section 4, the analysis is carried out for both angular and parallel misalignments and for different acceleration values.

When the speed of rotation is changing, the angular velocity can be taken as $\dot{\theta}(t) = \Omega_0 t + 1/2(at^2)$, where a is the angular acceleration of the rotor, Ω_0 is the initial angular velocity and t is the time. The Houbolt time marching technique is used to model the system in the time domain with a time step of 0.001 s, owing to better convergence of results [**23**]. The time response has been modelled until the system passes the critical speed. The Morlet mother wavelet [**24**] with a support length of $(-4, 4)$ has been chosen in the present study for all the CWTs. The centre frequency, ω_0, and bandwidth, $\Delta\omega$,

Downloaded from pic.sagepub.com at COLUMBIA UNIV on February 3, 2015

Table 1 Rotor–coupling–bearing system data

Acceleration of the rotor, a	20–70 rad/s^2
Torque, Tq	30 N m
First critical speed of rotor–coupling–bearing system (frictionless joint coupling)	1618 r/min (26.98 Hz)
First critical speed of rotor–coupling–bearing system (joint with stiffness and damping)	1516.2 r/min (25.27 Hz)
Shaft	
Diameter, D	20 mm
Density and modulus of elasticity	7800 kg /m^3, 2.08×10^{11} N/m^2
Disc	
Mass, m	5.5 kg
Polar moment of inertia, I_P	0.01546 kg m^2
Diametral moment of inertia, I_D	0.00773 kg m^2
Unbalance eccentricity, e	0.01 mm
Bearing (isotropic)	
Stiffness	2.5×10^5 N/m
Damping	100 N s/m
Coupling	
Type	Diaphragm coupling
Outer diameter	50 mm
Centre of articulation, Z_3	75.15 mm
Bending spring rate per degree per disc pack, K_b	30 N m/deg/disc pack
Rotational spring stiffness of coupling joint, $\bar{k}$	6.52×10^6 N m
Internal damping coefficient of coupling joint, $\bar{d}_i$	1000 N ms
Parallel misalignment	
$\Delta X1$	0.3–0.9 mm
$\Delta Y1$	0.3–0.9 mm
Angular misalignment, θ_3	0.1°–0.9°

of the mother wavelet, $\psi(t)$, in the frequency domain can be calculated by

$$\omega_0 = \frac{\int_{-\infty}^{\infty} \omega |\psi(\omega)|^2 \, d\omega}{\int_{-\infty}^{\infty} |\psi(\omega)|^2 \, d\omega} \tag{12}$$

$$\Delta\omega = \sqrt{\frac{\int_{-\infty}^{\infty} (\omega - \omega_0)^2 |\psi(\omega)|^2 \, d\omega}{\int_{-\infty}^{\infty} |\psi(\omega)|^2 \, d\omega}} \tag{13}$$

where $\psi(\omega)$ is the Fourier transform of $\psi(t)$.The centre frequency of daughter wavelets can be obtained by dividing the centre frequency of the mother wavelet by scale, ω_0/s.

The scale of the CWT should be chosen so that the centre frequency of the daughter wavelet in the frequency domain does not coincide with the critical and subcritical speeds. If the centre frequency of the daughter wavelet coincides with the critical speeds, the CWT coefficients at those speeds will be high and will not show the details at the other significant speeds. From the above expression of ω_0, the centre frequency of the Morlet mother wavelet can be calculated as 500 Hz (since the time step is 1 ms). The scale 35 has been chosen for all the CWTs since the centre frequency of the daughter wavelet (14.3 Hz) will not coincide with the critical and subcritical speeds (see Table 1 for the critical speed of the rotor system).

Figure 4 shows the time response and the corresponding CWT plots for a typical rotor–coupling–bearing system with and without misalignments. In this case a flexible coupling with a frictionless joint is considered. Clear change in the pattern of time response is observed in both systems with angular misalignment and parallel misalignment when compared with the system without misalignment. However, no clear features are noted in the time responses. In the case of CWT coefficient plots, the subharmonic resonant peaks at one-half, one-third and one-fourth the critical speed are evident when the misalignment is present in the system. These subcritical speeds are not observed in the time response as well as in the CWT plot when the rotor–coupling–bearing system is free from misalignment.

Similarly, the time response and the corresponding CWT plots are shown in Fig. 5 for the same rotor–coupling–bearing system with a flexible coupling having a joint with stiffness and damping. The critical and subcritical speeds (one-half, one-third and one-fourth the critical speed) are observed in CWT plots when misalignment is present (see Figs 5iib and 5iiib) as in the previous case. However, the critical speeds in the two cases are different: 1618 r/min (26.98 Hz) for a coupling with a frictionless joint and 1516.2 r/min (25.27 Hz) for a coupling having a joint with stiffness and damping (see Figs 4 and 5). A coupling with a frictionless joint is radially stiff and hence is more rigid compared with a coupling having a joint with stiffness and damping. For this reason, the critical speed of the rotor–coupling–bearing system with a frictionless joint is higher than that of a system having a joint with stiffness and damping. The amplitudes of vibration in the case of a system with a frictionless joint are low because of its radially stiff nature.

The variations in CWT coefficients at critical and subcritical speeds for the coupling with the two types of joint for angular and parallel misalignments are shown in Fig. 6. Equal amounts of misalignment in the x and y directions have been made in the case of parallel misalignment. All the subcritical speed curves start from (0, 0) in graphs since they are not present when the rotor system has no misalignment. The variation in the wavelet coefficients at critical and subcritical speeds is linear with angular and parallel misalignments for both cases of couplings. However, the rate of change in variation in wavelet coefficients with angular misalignment is high for a rotor–coupling–bearing system with a coupling joint having stiffness and damping. This is because the angular misalignment induces considerable moments at the joint, which make the joint flexible in nature when compared with a system with a frictionless joint (see

Downloaded from pic.sagepub.com at COLUMBIA UNIV on February 3, 2015

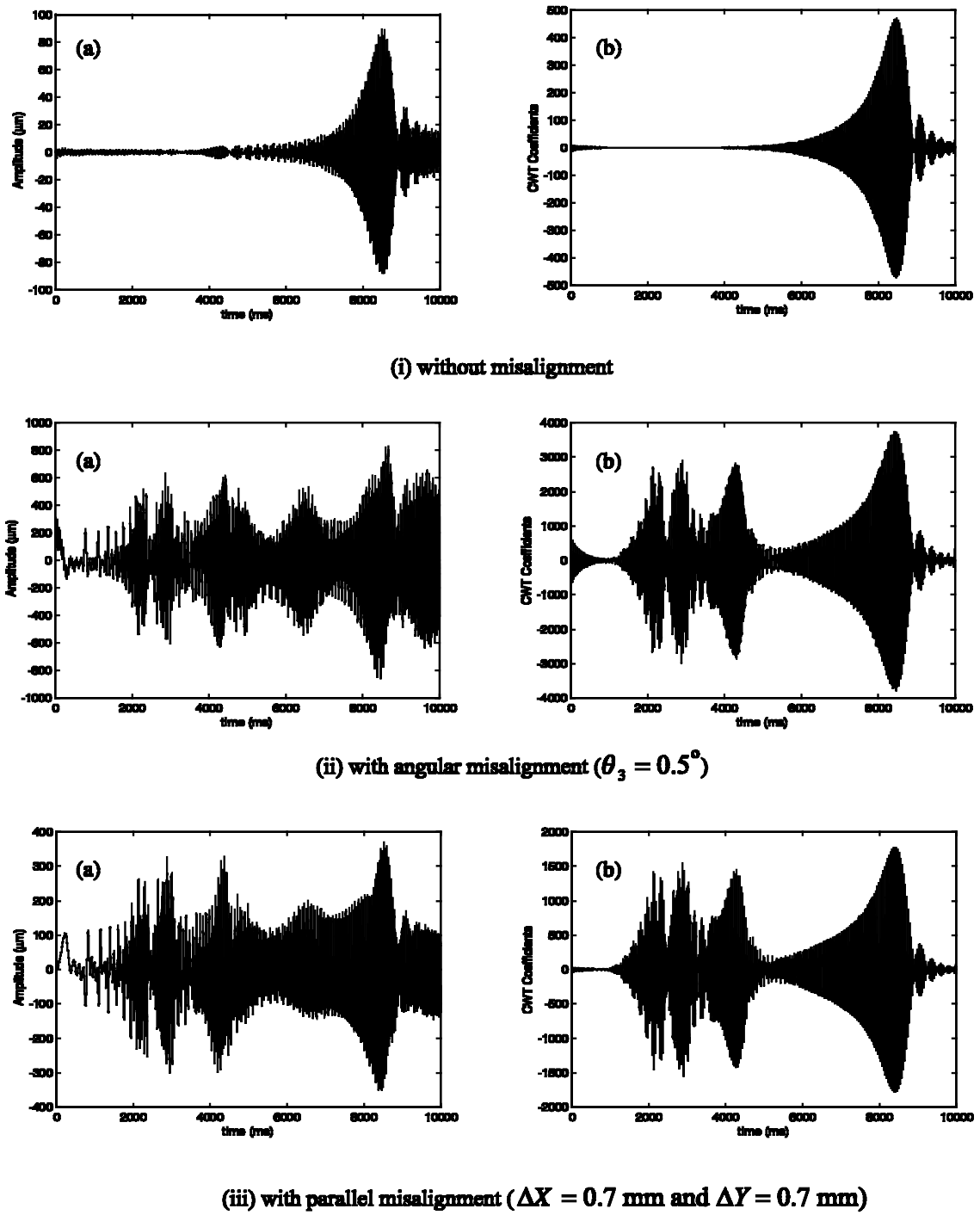

Fig. 4 Time response and CWT coefficients plot of a rotor system with a coupling having a frictionless joint ($a = 20\,\text{rad/s}^2$): (i) without misalignment, (ii) with angular misalignment ($\theta_3 = 0.5^{\circ}$) and (iii) with parallel misalignment ($\Delta X = 0.7\,\text{mm}$ and $\Delta Y = 0.7\,\text{mm}$) for (a) time and (b) CWT

Figs 6ia and iia). However, this rate is nearly equal in the case of parallel misalignment for both models of coupling (see Figs 6ib and iib). This is because the induced moments in the second model are negligible since angular effects are not present.

The time response and CWT coefficients have been plotted in Fig. 7 for different angular accelerations of a misaligned rotor–coupling–bearing system with a frictionless joint. At low angular accelerations, the critical and all the subcritical speeds are clear in the CWT plot (see Fig. 7a). However, as the angular acceleration increases, the subcritical speeds at one-third and one-fourth the critical speeds merge (see Figs 7b and c) because the time available to pass the two subcritical

Downloaded from pic.sagepub.com at COLUMBIA UNIV on February 3, 2015

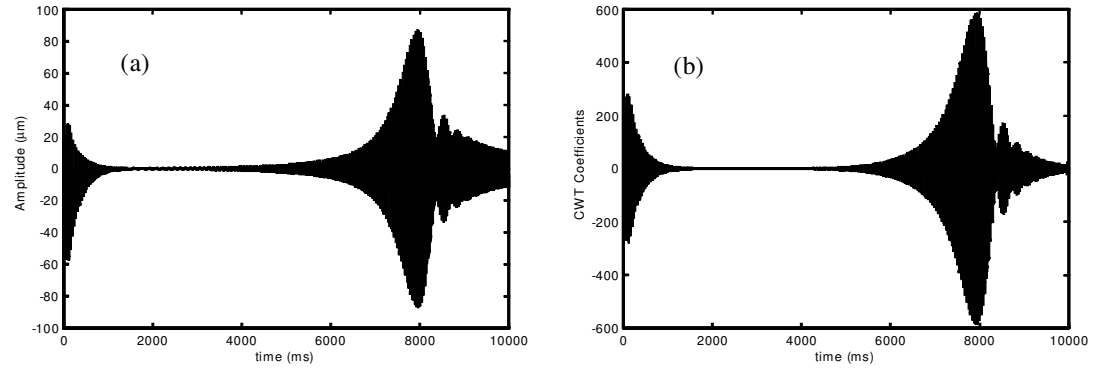

(i) without misalignment

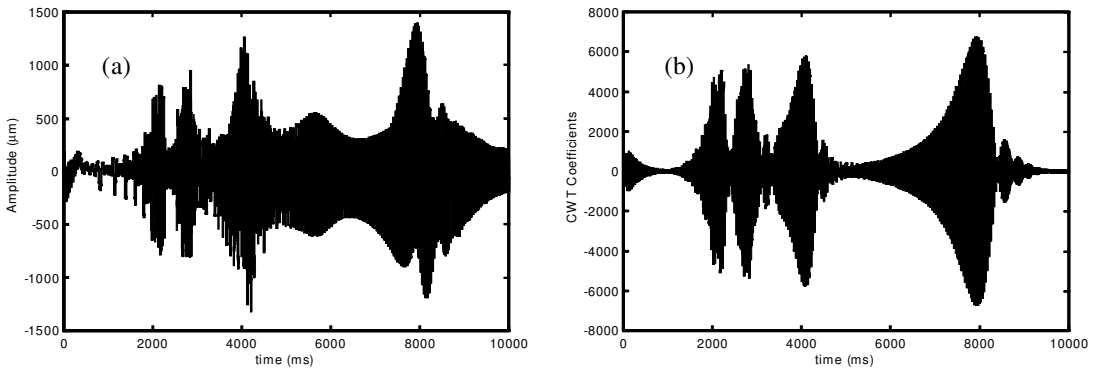

(ii) with angular misalignment ($\theta_3 = 0.5^{\circ}$)

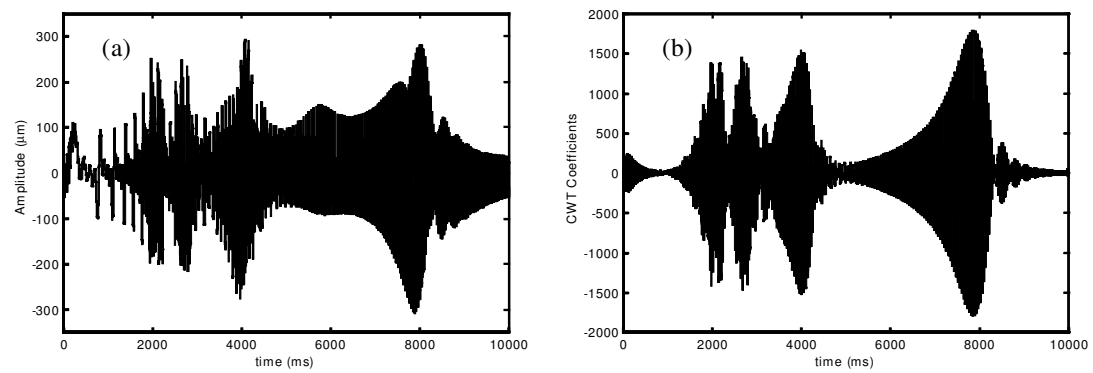

(iii) with parallel misalignment ($\Delta X = 0.7$ mm and $\Delta Y = 0.7$ mm)

Fig. 5 Time response and CWT coefficients plot of a rotor system with a coupling having a joint with stiffness and damping ($a = 20\,\mathrm{rad/s^2}$): (i) without misalignment, (ii) with angular misalignment ($\theta_3 = 0.5^{\circ}$) and (iii) with parallel misalignment ($\Delta X = 0.7$ mm and $\Delta Y = 0.7$ mm) for (a) time and (b) CWT

speeds is low. It can also be observed from the figures that at high angular accelerations the vibration amplitudes are less. This can be expected since the increase in driving torque reduces the vibration owing to the shorter time needed to pass through the critical and subcritical speed region.

Recently, the use of large rotating machines which start and stop quite frequently has increased. In such machines, vibration monitoring during start-up or shutdown is as important as the steady state to detect coupling misalignment. The present analysis helps to detect coupling misalignment at early stages

Downloaded from pic.sagepub.com at COLUMBIA UNIV on February 3, 2015

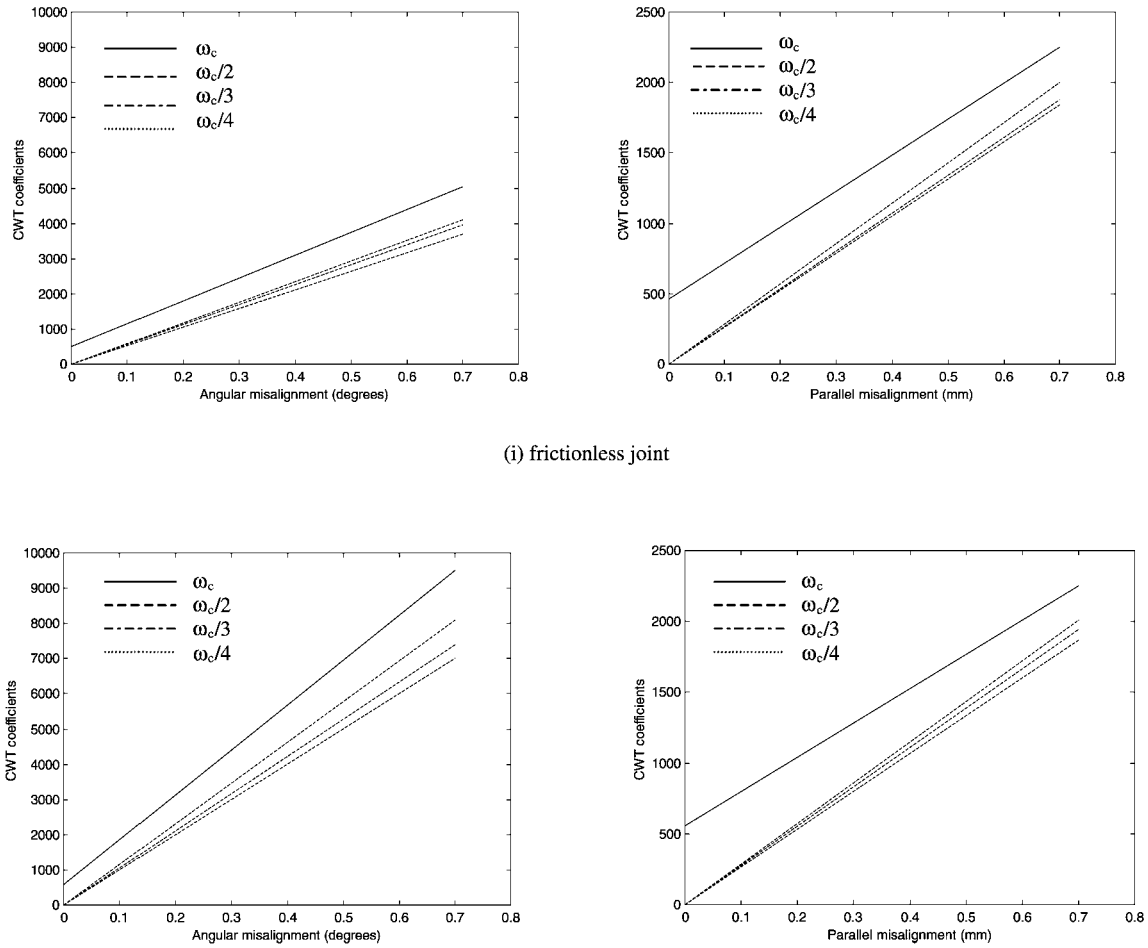

Fig. 6 Variation in wavelet coefficients at critical and subcritical speeds of a rotor–coupling–bearing system with misalignment ($a = 20\,\mathrm{rad/s^2}$): (i) frictionless joint and (ii) joint with stiffness and damping for (a) angular misalignment and (b) parallel misalignment

of the machine operation (before reaching the steady state).

7 CONCLUSIONS

The transient response of a misaligned rotor coupling–bearing system has been analysed by using FEM analysis for flexural vibrations. The analysis has been carried out by considering two different coupling models, one with a frictionless joint and the other with a joint with stiffness and damping.

The CWT is found to be a useful tool for feature extraction from the time response of the misaligned rotor coupling–bearing system. The subcritical speeds at one-half, one-third and one-fourth the critical speed are found in CWT coefficient plots when misalignment is present in the rotor system. It is observed that the critical speed of the rotor–bearing system having a coupling with a frictionless joint is higher than that of a joint with stiffness and damping. It is also observed that the variations in CWT coefficients at critical as well as subcritical speeds with misalignment are linear. Moreover, the rate of change in CWT coefficients with angular misalignment is higher for the rotor system having a coupling with a joint having stiffness and damping, as compared with the other model.

At low angular accelerations, the critical and all the subcritical speeds are clear in the CWT plot. It is noticed that at high angular acceleration the subcritical speeds at one-third and one-fourth the critical speeds merge because the time available to pass the two subcritical speeds is short.

The present analysis of CWT can be used to detect coupling misalignment at the early stages of machine operation before reaching the steady state. More

Downloaded from pic.sagepub.com at COLUMBIA UNIV on February 3, 2015

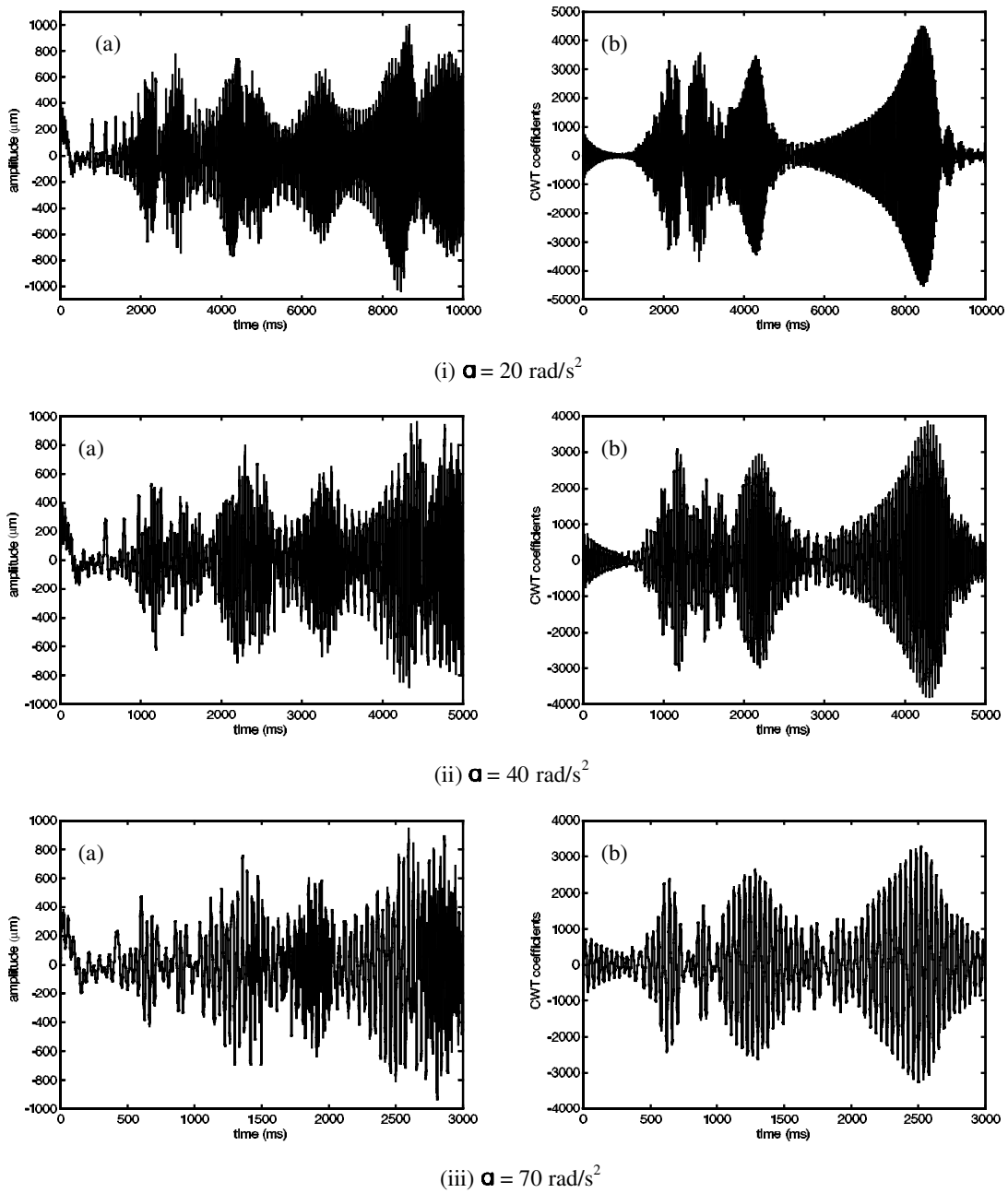

Fig. 7 Time response and CWT coefficients plot of a misaligned rotor coupling–bearing system having a frictionless joint for different accelerations ($\theta_3 = 0.6$): (i) $a = 20\,\text{rad/s}^2$, (ii) $a = 40\,\text{rad/s}^2$ and (iii) $a = 70\,\text{rad/s}^2$ for (a) time and (b) CWT

theoretical analysis with experimental validation on coupling misalignments is essential where limited work has been done. Such work will be carried out in the future.

REFERENCES

1 **Xu, M.** and **Marangoni, R. D.** Flexible couplings: study and application. *Shock and Vibr. Dig.*, 1990, **22**(9), 3–11.

2 **Rivin, E. I.** Design and application criteria for connecting couplings. *Trans. ASME, J. Mechanisms, Transm. Automn Des.*, 1986, **108**, 96–104.

3 **Woodcock, J. S.** The effects of couplings upon the vibrations of the rotating machinery. In Proceedings of International Conference on *Flexible Couplings*, University of Sussex, Brighton, 1977, pp. E-1-1–E-1-20 (Michael Neale and Associates Limited).

4 **Gibbons, C. B.** Coupling misalignment forces. In Proceedings of 5th Turbomachinery Symposium, Gas Turbine Laboratories, Texas A&M University, Texas, 1976, pp. 111–116.

5 **Arumugam, P., Swarnamani, S.** and **Prabhu, B. S.** Effects

Downloaded from pic.sagepub.com at COLUMBIA UNIV on February 3, 2015

of coupling misalignment on the vibration characteristics of a two stage turbine rotor. *ASME Des. Engng Tech. Conf.*, 1995, **84**, 1049–1054.

6 **Sekhar, A. S.** and **Prabhu, B. S.** Effects of coupling misalignment on vibrations of rotating machinery. *J. Sound Vibr.*, 1995, **185**(4), 655–671.

7 **Dewell, D. L.** and **Mitchell, L. D.** Detection of a misaligned disk coupling using spectrum analysis. *Trans. ASME, J. Vibr., Acoust., Stress and Reliability in Des.*, 1984, **106**, 9–15.

8 **Maten, S.** Program machine maintenance by measuring vibration velocity. *Hydrocarbon Processing*, 1970, **49**(9), 291–296.

9 **Piotrowski, J.** *Shaft Alignment Hand Book* (Marcel Dekker, New York and Basel).

10 **Xu, M.** and **Marangoni, R. D.** Vibration analysis of a motor–flexible coupling rotor–system subjected to misalignment and unbalance, Part I: theoretical model and analysis. *J. Sound Vibr.*, 1994, **176**(5), 663–679.

11 **Xu, M.** and **Marangoni, R. D.** Vibration analysis of a motor–flexible coupling–rotor system subjected to misalignment and unbalance, Part II: experimental validation. *J. Sound Vibr.*, 1994, **176**(5), 681–691.

12 **Sekhar, A. S.** and **Srinivasa Rao, A.** Vibration analysis of rotor–coupling bearing system with misaligned shafts. In 41st ASME International Gas Turbines and Aeroengine Congress and Exhibition, Birmingham, 1996, paper 96-GT-12.

13 **Sekhar, A. S.** and **Srinivasa Rao, A.** Crack versus misalignment in rotor–coupling bearing system. *J. Mach. Vibr.*, 1996, **5**, 179–188.

14 **Lee, Y. S.** and **Lee, C. W.** Modelling and vibration analysis of misaligned rotor–ball bearing systems. *J. Sound Vibr.*, 1999, **224**(1), 17–32.

15 **Newland, D. E.** Wavelet analysis of vibration, part I: theory. *Trans. ASME, J. Vibr. Acoust.*, 1994, **116**(4), 409–416.

16 **Newland, D. E.** Wavelet analysis of vibration, part II: wavelet maps. *Trans. ASME, J. Vibr. Acoust.*, 1994, **116**(4), 417–425.

17 **Staszewski, W. J.** Structural and mechanical damage detection using wavelets. *Shock Vibr. Dig.*, 1998, **30**(6), 457–472.

18 **Wang, W. J.** and **McFadden, P. D.** Application of wavelets to gearbox vibration signals for fault detection. *J. Sound Vibr.*, 1996, **192**(5), 927–939.

19 **Prabhakar, S., Sekhar, A. S.** and **Mohanty, A. R.** Detection and monitoring of cracks in a rotor–bearing system using wavelet transforms. *J. Mech. Systems and Signal Processing*, 2001, **14** (in press).

20 **Nelson, H. D.** and **McVaugh, J. M.** The dynamics of rotor–bearing systems using finite elements. *Trans. ASME, J. Engng for Industry*, 1976, **98**(2), 593–600.

21 **Ozguven, H. N.** and **Ozkan, Z. L.** Whirl speeds and unbalance response of multibearing rotor using finite elements. *Trans. ASME, J. Vibr., Acoust., Stress and Reliability in Des.*, 1984, **106**, 72–79.

22 **Kramer, E.** *Dynamics of Rotors and Foundations*, pp. 224–226 (Springer-Verlag, Berlin).

23 **Subbiah, R.** and **Reiger, N. F.** On the transient analysis of rotor–bearing systems. *Trans. ASME, J. Vibr., Acoust., Stress and Reliability in Des.*, 1988, **110**, 515–520.

24 **Daubechies, I.** *Ten Lectures on Wavelets*, 1994, Vol. 61, p. 76 (CBMS, SIAM).

Downloaded from pic.sagepub.com at COLUMBIA UNIV on February 3, 2015